Catalysis Science & Technology

Accepted Manuscript

ROYAL SOCIETY OF CHEMISTRY

www.rsc.org/catalysis

Journal Name

ARTICLE

Role of FeO_x support in constructing high performance Pt/FeO_x catalyst for low-temperature CO oxidation

Received 00th January 20xx,
Accepted 00th January 20xx

DOI: 10.1039/x0xx00000x

www.rsc.org/

Bin Zheng,[a] Gang Liu*, [a] Longlong Geng, [a] Junyan Cui, [a] Shujie Wu, [a] Ping Wu, [a] Mingjun Jia, [a] Wenfu Yan [b] and Wenxiang Zhang* [a]

Based on a simple colloid deposition method, a series of Pt/FeO_x catalysts were prepared using 3–4 nm Pt colloid nanoparticles and FeO_x with different microstructure (i.e. the structure and surface properties). FeO_x support was obtained via a thermal-treatment method, which enables the tailoring of FeO_x from ferrihydrite to α-Fe_2O_3 and the amount of hydroxides on the surface of FeO_x decreases gradually with the phase changing. Over an optimized Pt/FeO_x, CO could be completely converted at room temperature (298 K) and a relatively high space velocity (1.2×10^5 $mL\cdot g^{-1}\cdot h^{-1}$). The correlation between the microstructure of FeO_x support and the CO oxidation performance of resultant Pt/FeO_x catalyst was investigated. Although the oxidation of Pt nanoparticles is inevitable in the process of Pt-loading, relatively large amounts of Pt^0 species can be preserved on the FeO_x support possessing abundant surface hydroxides. In-situ DRIFT shows that the surface hydroxides of FeO_x could also participate in the catalytic process: they could react with CO absorbed on Pt^0 sites and then recover easily in the co-presence of molecular oxygen and water gas. These results show that intrinsic properties of FeO_x support not only affect the oxidation state of supported Pt nanoparticles in the preparation process, but also provide new active sites in the catalytic process. FeO_x support possessing abundant surface hydroxides is suitable for preparing high performance Pt/FeO_x catalyst for low-temperature CO oxidation.

Introduction

Nowadays supported Pt nanoparticles are a kind of efficient heterogeneous catalysts used in many hydrogenation and oxidation reactions.[1-4] But in a very long period of time, supported Pt catalysts were considered inert in low-temperature CO oxidation.[5-8] The barrier to this catalytic process is the strongly adsorbed CO onto Pt, which inhibits O_2 adsorption and hinders CO_2 formation.[9-11] Recent progress shows that this barrier could be significantly decreased via constructing an efficient Pt-support interface using reducible metal oxides as supports.[12-14]

Among various adopted reducible metal oxides, iron oxide (FeO_x) was proved to be favourable for preparing high-performing supported Pt catalysts for low-temperature CO oxidation.[15-22] Two earlier successful works were individually reported by Deng et al.[19] and our group[18] through adopting suitable preparation method. The optimized Pt/FeO_x catalyst exhibits a superior long-term stability. The total conversion of CO could be maintained for more than 3000 h at 25°C in the presence of water vapour (space velocity is 1.2×10^4 $mL\cdot g^{-1}\cdot h^{-1}$).[18] The intrinsic properties of FeO_x should have an important influence on the formation of the efficient Pt-support interface. However, the questions of what the key factor is in controlling the formation of Pt-FeO_x interface, and how it works in the preparation process, are still unclear. Based on conventionally co-precipitation method, the support effect of FeO_x cannot be easily distinguished from the composite system.[19, 20] The Pt particle size, microstructure of FeO_x support and the Pt-support interface are all changing during the thermal or redox treatment, which makes the influence factors much complex.

Besides, how the FeO_x supports participate in the CO oxidation (i.e., activate molecular oxygen) is also under debate. Some work reported that the lattice oxygen of FeO_x support should participate in the CO oxidation, and proposed that the reaction over Pt/FeO_x follows the redox mechanism (Mars-van Krevelen mechanism).[3, 12, 23] A few researches thought that the CO oxidation over Pt/FeO_x follows a Langmuir-Hinshelwood mechanism. Oxygen molecularly adsorbs onto the oxygen vacancy of the FeO_x support, and reacts with CO adsorbed onto Pt sites.[9, 20, 24] Therefore, further clarifying the effect of FeO_x on both the preparation and catalytic process is quite desirable for rational design of high performance supported Pt catalysts.

The colloid deposition method provides an opportunity to clarify the support effect of FeO_x in Pt/FeO_x catalyst. The Pt colloid was generated before the addition of the support.[18] The size of Pt nanoparticles could be preserved after the deposition onto the support. Thus, the effect of Pt size could be nearly avoided when using the same Pt colloid to prepare Pt/FeO_x catalysts.[21] The support

[a] Key Laboratory of Surface and Interface Chemistry of Jilin Province, College of Chemistry, Jilin University, Changchun, 130012, China
[b] State Key Laboratory of Inorganic Synthesis and Preparative Chemistry,College of Chemistry, Jilin University, Changchun, 130012, China
*Email: lgang@jlu.edu.cn (Gang Liu), zhwenx@jlu.edu.cn (Wenxiang Zhang)
Tel: (+86)431-85155390 Fax: (+86)431-88499140
Electronic Supplementary Information (ESI) available: [details of any supplementary information available should be included here]. See DOI: 10.1039/x0xx00000x

effect of FeO_x on the preparation and catalytic processes of Pt/FeO_x can be discussed separately. In this work, a series of Pt/FeO_x catalysts were prepared by the colloid deposition method using FeO_x with different microstructure (i.e., the structure and surface properties) as supports. The FeO_x were obtained via thermal treating a ferric hydroxide precursor at different temperature. Under an optimized condition, CO could be completely converted over Pt/FeO_x catalyst at room temperature (298 K) and a relatively high space velocity (1.2×10^5 $mL \cdot g^{-1} \cdot h^{-1}$). System characterizations, including in-situ DRIFT, were carried out to investigate the physico-chemical properties of both FeO_x and Pt/FeO_x. The role of FeO_x in the formation of Pt-support interface and the process of molecular oxygen activation was discussed based on these characterization results.

Experimental

Materials

All chemical reagents were obtained from commercial sources and used without further purification. Hexachloroplatinic(IV) acid hexahydrate was purchased from Sinopharm Chemical Reagent Co.,Ltd.

Catalyst Preparation

The precursor of FeO_x support was prepared with a precipitation method using $Fe(NO)_3 \cdot 9H_2O$ as the iron source and Na_2CO_3 as the precipitation agent. Typically, 56 g $Fe(NO)_3 \cdot 9H_2O$ was dissolved in 50 mL water. Na_2CO_3 aqueous solution (0.22 M) was added to adjust the pH value to 9.0 and the mixture was filtered with a Buchner funnel. The solid was dried at 100 °C for 0.5 h to obtain the precursor. Different FeO_x support was prepared by calcinating the precursor at desired temperatures for 1.5 h in a flow of 20% O_2/Ar. The calcination temperatures were determined on the basis of TG-DTA characterization (Fig. 1) and the resultant materials were denoted as FeO_x-T (T = 100, 130, 220, 300, 430, 500).

Pt colloids were prepared with a polyol reduction method.[18, 25] The detailed procedure is as following: 27 mL glycol solution of sodium hydroxide (0.34 M) was dropwise added into 60 mL glycol solution of $H_2PtCl_6 \cdot 6H_2O$ (8.5×10^{-4} M) under a continuous stir. The resultant solution was heated at 140 °C for 30 min under the protection of Ar atmosphere and then black Pt colloids were obtained.

The Pt/FeO_x-T catalysts were prepared by a colloid deposition method described previously.[18, 21] FeO_x-T support was mixed with Pt colloids and heated at 80 °C under moderate stirring until the deposition of Pt colloids were totally finished. The content of Pt in the final Pt/FeO_x-T catalysts is 1 wt %. The resultant solid was isolated and washed thoroughly with distilled water until there are no chloride ions ($AgNO_3$ test). The products were dried at 100 °C overnight and then calcined at 200 °C for 2 h in a flow of 20% O_2/Ar.

Catalyst Characterization

Thermogravimetry and differential thermogravimetry (TG-DTA) measurements were performed using NETZSCH STA 449c thermal station with a heating rate of 10 $°C \cdot min^{-1}$. Powder X-ray diffraction (XRD) patterns were recorded on a Rigaku X-ray diffractometer using Cu Kα radiation (k = 1.5418 A). N_2 adsorption/desorption isotherms were measured at 77 K, using a Micromeritics ASAP 2010N analyzer. Samples were degassed at 373 K for 20 h before measurements. Specific surface areas were calculated using the Brunauer-Emmett-Teller (BET) model. Pore size distributions were evaluated from adsorption branches of nitrogen isotherms using the Barret-Joyner-Halenda (BJH) model. X-ray photoelectron spectroscopy (XPS) was performed on a Thermo ESCA LAB 250 system with Mg Kα source (1254.6 eV). The XPS spectra were calibrated by adjusting the C 1s peak to a position of 284.6 eV. Transmission electron microscopy (TEM) observations were carried out on a JEOL JEM-2010 electron microscope with an operating voltage of 200 kV. Scanning electron microscopy (SEM) images were taken on a Hitachi S-5500. Temperature programmed hydrogen reduction (H_2-TPR) was performed with a homemade equipment. The samples were pretreatment in Ar (99.99%) at 120 °C for 30 min and then exposed to a stream of 5 vol % H_2/Ar at 25 °C. A heating rate of 10 $°C \cdot min^{-1}$ was used in these experiments. The uptake amount of H_2 during the reduction was measured using a Shimadzu GC-8A chromatograph equipped with a thermal conductivity detector (TCD). In-situ DRIFT spectra were recorded on a Nicolet 6700 spectrometer. Initially, each sample was finely ground and placed in a ceramic crucible; the sample was pretreated in Ar at 25 °C for 20 min and was then exposed to a stream of 1 vol % CO/Ar. After turning off the stream of 1 vol % CO/Ar, 10 vol % O_2/Ar was introduced. 1 vol % CO/Ar and 10 vol % O_2/Ar were introduced in the ceramic crucible to monitor the whole process by the spectrometer, and all spectra were recorded with a resolution of 4 cm^{-1} and comprise 32 averaged, background subtracted scans.

Catalytic test

The catalytic oxidation activity of CO was measured using a continuous-flow fixed-bed reactor system. The Pt/FeO_x-T samples were directly used without further reduction treatment. 50 mg of solid catalyst sample (40–60 mesh) was loaded between two glass wool beds in a quartz tube reactor. The gas mixture consisted of 0.5% CO and 10% O_2, balanced with Ar. The total flow rate is 100 $mL \cdot min^{-1}$. Kinetic data were taken after 10 min on stream at each reaction temperature. The products analysis was carried out using a Shimadzu GC-8A gas chromatograph equipped with a TCD.

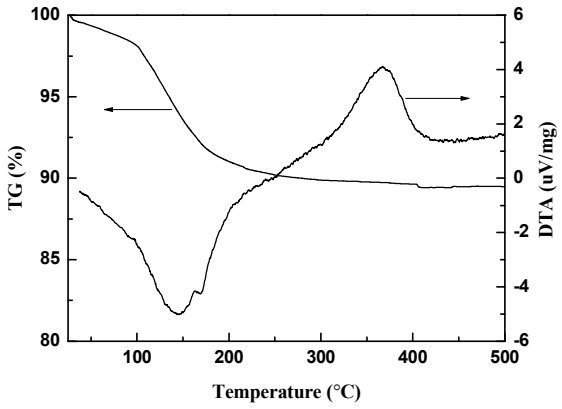

Fig. 1 TG-DTA curves of as-synthesized FeO_x precursor.

Results and discussion

Preparation and characterization of FeO_x supports

As described in Experimental section, different FeO_x supports were obtained by thermal-treating a ferric hydroxide precursor prepared with a precipitation method. The desired treating temperatures were determined on the basis of TG-DTA characterization (Fig. 1). In TG curve, a weight loss of ca. 2% can be observed from room temperature to 100 °C, and a significant weight loss of ca. 8% occurs in the range of 100 to 220 °C. The latter stage accompanies with a strong endothermic peak, corresponding to the expulsion of water in the thermal-treated process.[26] The obvious phase transformation should occur between 250 and 430 °C. A strong exothermic peak (centre at 366 °C) with a small shoulder (at 290 °C) can be observed in this range. Based on these results, the thermal-treating temperatures of 100, 130, 220, 300, 430 and 500 °C were adopted in this work, aiming to obtain FeO_x supports with different structures and surface properties.

XRD patterns show that FeO_x-100 possesses two broad diffraction peaks at 2θ = 35 and 62.5 °, which are typical two-line patterns of ferrihydrite ($FeO(OH, H_2O)_n$, Fig. 2).[19, 26] As for FeO_x-130 and FeO_x-220, five additional diffraction peaks at 2θ = 35.6, 40.8, 49.5, 54.1, 63.9 ° can be observed, which can be ascribed to the diffraction of hematite (α-Fe_2O_3, PDF card No.33-0664). It shows the co-presence of $FeO(OH, H_2O)_n$ and α-Fe_2O_3 in the samples of FeO_x-130 and FeO_x-220.[27] The intensity of α-Fe_2O_3 peak is very low, suggesting that the crystallization of α-Fe_2O_3 is not very well or the amount of α-Fe_2O_3 is limited. As for FeO_x-300, all of the diffraction peaks could be indexed to α-Fe_2O_3. The dominant peaks at 33.1, 35.6, 54.1° are corresponding to (104), (110), and (116) diffraction peaks of α-Fe_2O_3. With the treating temperature increasing to 430 and 500 °C, the intensity of diffraction peaks indexed to α-Fe_2O_3 further increased, indicating α-Fe_2O_3 is the main phase in the samples of FeO_x-430 and FeO_x-500.[28] The BET surface areas of these samples also exhibit a gradual change with the increase of treating temperature, decreasing from 185 $m^2 \cdot g^{-1}$ of FeO_x-100 to 41 $m^2 \cdot g^{-1}$ of FeO_x-500 (Table S1). SEM images show that the morphologies of these FeO_x samples have no obvious difference. There are no large

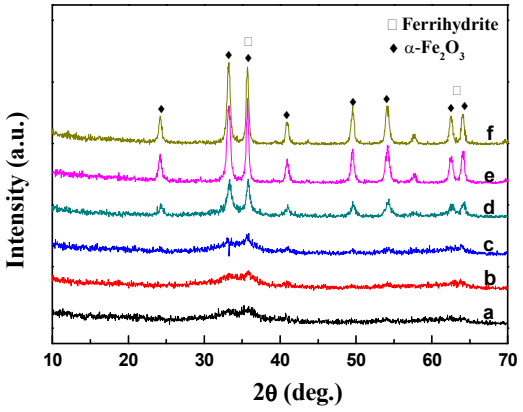

Fig. 2 XRD patterns of FeO_x supports: (a) FeO_x-100, (b) FeO_x-130, (c) FeO_x-220, (d) FeO_x-300, (e) FeO_x-430 and (f) FeO_x-500.

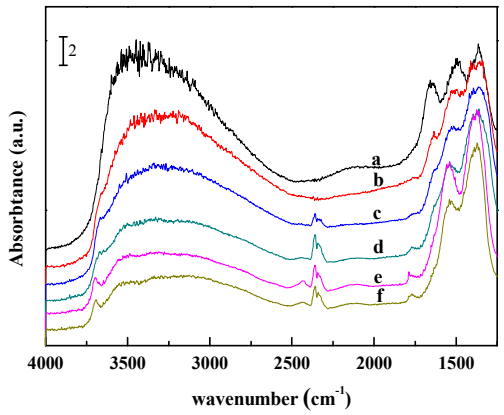

Fig. 3 DRIFT spectra of FeO_x supports: (a) FeO_x-100, (b) FeO_x-130, (c) FeO_x-220, (d) FeO_x-300, (e) FeO_x-430 and (f) FeO_x-500.

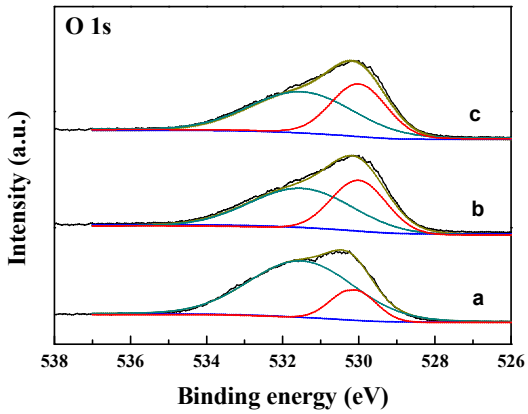

Fig. 4 O 1s XPS spectrum of FeO_x supports: (a) FeO_x-100, (b) FeO_x-300, (c) FeO_x-500.

crystals present in the FeO_x-430 and FeO_x-500 samples (Fig. S1).

DRIFT spectra of these iron oxide samples are shown in Fig. 3. The band at about 2330 cm^{-1} can be attributed to the stretching vibration of CO_2, the band at about 1496 cm^{-1} and 1373 cm^{-1} should be due to superposition of carbonate and nitrate species.[29] The broad absorption bands at 3400 and 1620 cm^{-1} could be attributed to normal polymeric O-H stretching vibration of H_2O present in these samples.[26, 29, 30] The absorption band at 3695 cm^{-1} is assigned to the stretching vibration of surface OH. The intensities of these three bands decrease with the increase of treating temperature. It suggests that the amount of both surface OH and structural OH decreases with the increase of treating temperature. These phenomena were further supported by O 1s XPS analysis. As shown in Fig. 4, it can be fitted by the presence of OH (531.5 eV) and bridging O groups (529.8 eV).[31, 32] The OH/O ratio decreases from 4:1 of FeO_x-100 to 1:1 of FeO_x-500.

H_2-TPR profiles show that these iron oxide samples possess three reduction peaks (Fig. 5). The former two peaks in the region of 300–400 °C and 400–550 °C can be corresponding to the reduction of $FeO(OH, H_2O)_n/Fe_2O_3$ to Fe_3O_4 and some FeO species. The broad peak located at above 600 °C is corresponding to the further

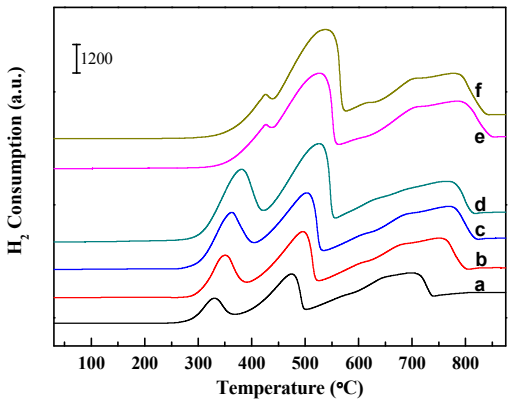

Fig. 5 H_2-TPR profiles of FeO_x supports: (a) FeO_x-100, (b) FeO_x-130, (c) FeO_x-220, (d) FeO_x-300, (e) FeO_x-430 and (f) FeO_x-500.

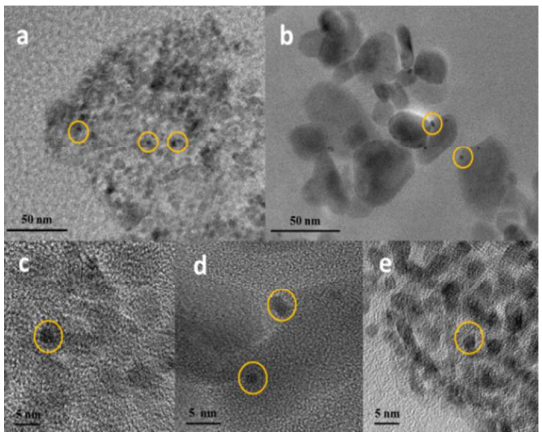

Fig. 7 TEM and HRTEM images of Pt/FeO_x-100 (a) (c), Pt/FeO_x-500 (b) (d) and Pt colloids (e).

reduction to FeO/Fe species.[33] The reduction peak gradually shifts to relatively high temperature with the treating temperature increasing from 100 to 500 °C.

Role of FeO_x microstructure in the formation of Pt-support interface

The Pt/FeO_x-T catalysts with 1 wt % Pt were prepared by a colloid deposition method. All the samples were calcined at 200 °C for 2 h in a flow of 20 vol % O_2/Ar before being used as catalysts and characterization. XRD patterns show that diffraction peaks ascribed to α-Fe_2O_3 obviously appear in the sample of Pt/FeO_x-100, Pt/FeO_x-130 and Pt/FeO_x-220 (Fig. 6). Two additional peaks at 30.1 and 43.1° can also be observed in the above three samples and Pt/FeO_x-300, which can be assigned to the formation of Fe_3O_4 phase. This phase transformation was confirmed by a Mössbauer spectra measurement (Fig. S3, Table S4). It shows that a solid state reaction should occur in these samples between Pt nanoparticles and FeO_x support. The crystal phase of FeO_x changes from ferrihydrite to α-Fe_2O_3 and is partly reduced to Fe_3O_4 after this solid state reaction. This process accompanies with the removal of hydroxyl groups on the surface of FeO_x (see in DRIFT spectra, Fig. S4).[34] As for Pt/FeO_x-430 and Pt/FeO_x-500, only α-Fe_2O_3 phase can be observed, indicating the interface reaction is very weak in these two samples. Besides, no Pt diffraction peaks can be observed in the XRD patterns of all catalysts, showing that the particle size of Pt should be quite small and highly dispersed on the surface of FeO_x. It was confirmed by HRTEM (Fig. 7) that Pt nanoparticles of 3–4 nm dispersed on the FeO_x surface. They nearly preserve the particle size of Pt colloid nanoparticles.

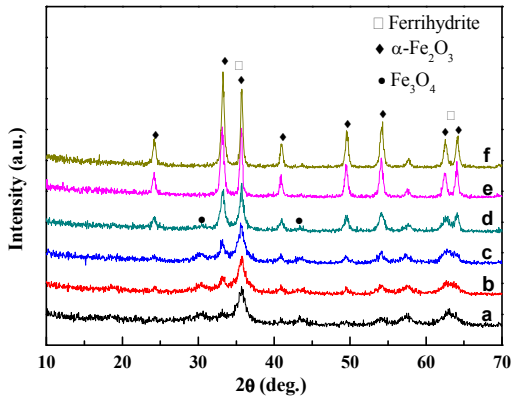

Fig. 6 XRD patterns of Pt/FeO_x catalysts: (a) Pt/FeO_x-100, (b) Pt/FeO_x-130, (c) Pt/FeO_x-220, (d) Pt/FeO_x-300, (e) Pt/FeO_x-430 and (f) Pt/FeO_x-500.

Fig. 8 shows the Pt 4f XPS spectra of the three representative samples Pt/FeO_x-100, Pt/FeO_x-300 and Pt/FeO_x-500. The main photoemission lines in the Pt 4f spectra recorded from Pt/FeO_x-300 and Pt/FeO_x-500 appear at higher binding energy than those of the spectrum of Pt/FeO_x-100, indicating the average Pt oxidation state in Pt/FeO_x-300 and Pt/FeO_x-500 is higher than that of Pt in Pt/FeO_x-100. The relatively broad curves can be fitted into two pairs of peaks assigned to Pt^{2+} (72.4, 75.6 eV) and Pt^0 (71.3, 74.7eV), respectively.[19, 35, 36] The molar ratio of Pt^{2+}/Pt^0 is 0.74, 1.54 and 1.64 for Pt/FeO_x-100, Pt/FeO_x-300 and Pt/FeO_x-500, indicating that the amount of Pt^{2+} increases from Pt/FeO_x-100 to Pt/FeO_x-500. Due to the low resolution of Pt 4f signal, reproduced experiments, including catalysts preparation and XPS characterization, were carried out to confirm the accuracy of above information. The results show that the above phenomena are reproducible. As described above, Pt/FeO_x catalysts were prepared by depositing Pt nanoparticles on the surface of FeO_x support, and calcined at 200 °C for 2 h in a flow of 20 vol % O_2/Ar. In the preparation process of Pt/FeO_x, part of Pt^{2+} should form from the oxidation of Pt nanoparticle by O_2. Since the preparation condition is the same for all Pt/FeO_x catalysts, the difference of Pt^{2+}/Pt^0 ratio among Pt/FeO_x catalysts should be correlated with the surface properties of FeO_x support. According to above characterization, it can be deduced that a solid state reduction-oxidation reaction should occur at the Pt-FeO_x interface in this preparation process. A certain amount of electrons transfers from Pt to the FeO_x support, forming Pt^{2+} species. This process is strongly dependent upon the microstructure of FeO_x support.[6] It has shown that the phase of FeO_x supports change from ferrihydrite to hematite phase with the thermal-treating temperature increasing. Surface hydroxyl groups decreased significantly from FeO_x-100 to

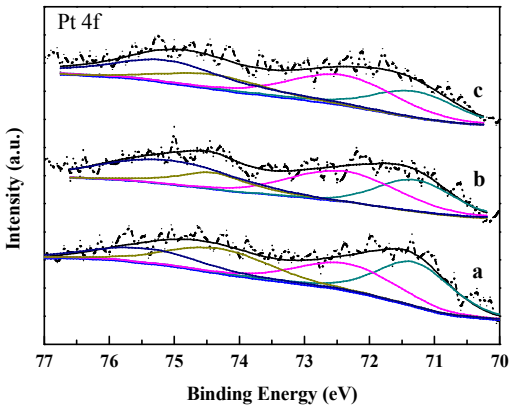

Fig. 8 Pt 4f XPS spectra of Pt/FeO_x catalysts: (a) Pt/FeO_x-100, (b) Pt/FeO_x-300, (c) Pt/FeO_x-500.

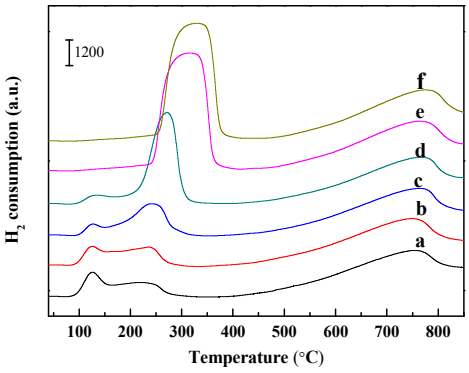

Fig. 9 H_2-TPR profiles of Pt/FeO_x catalysts: (a) Pt/FeO_x-100, (b) Pt/FeO_x-130, (c) Pt/FeO_x-220, (d) Pt/FeO_x-300, (e) Pt/FeO_x-430, (f) Pt/FeO_x-500.

FeO_x-500. It will accompany the formation of oxygen vacancy in the FeO_x treating at high temperature to maintain the charge balance of the system.[36, 37] In the process of Pt/FeO_x-100 preparation, with the assistance of Pt nanoparticle, a small portion of Fe^{3+} in the FeO_x-100 was reduced to Fe^{2+} forming a certain amount of Fe_3O_4 phase (see in XRD patterns, Figure 6). As for FeO_x treated at high temperature, Pt nanoparticles easily reside at the oxygen vacancies of FeO_x and more electrons transfer from Pt to FeO_x to neutralize the positive charge of these vacancies, leading to form relatively large amount of Pt^{2+} in Pt/FeO_x-300 and Pt/FeO_x-500. Relatively large amounts of Pt^0 species can be preserved on the FeO_x support possessing abundant surface hydroxides.

The reducibility of the Pt/FeO_x catalysts was measured by H_2-TPR (Fig. 9). Compared to FeO_x supports, a peak centered at much lower temperature (125 °C) was observed in the profiles of Pt/FeO_x-100, Pt/FeO_x-130, Pt/FeO_x-220 and Pt/FeO_x-300. The corresponding H_2 consumption amount is 1.04, 0.77, 0.40 and 0.31 mmol·g^{-1}, respectively (Table S5). This amount is much larger than that required for reducing Pt^{2+} to Pt^0, suggesting that Fe^{3+} species around Pt were also prone to be reduced.[37] This low-temperature peak is absent in the samples of Pt/FeO_x-430 and Pt/FeO_x-500. It reflects that Pt species interact strongly with FeO_x-430 and FeO_x-500 support. Besides, the area of this peak decreases from Pt/FeO_x-100 to

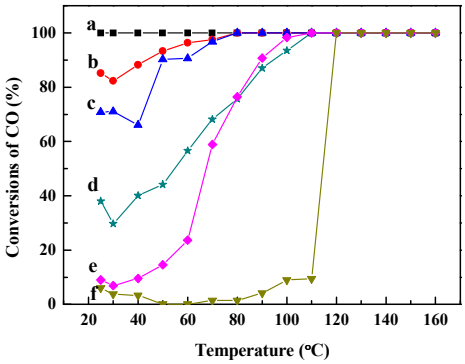

Fig. 10 CO catalytic oxidation activities of Pt/FeO_x catalysts: (a) Pt/FeO_x-100, (b) Pt/FeO_x-130, (c) Pt/FeO_x-220, (d) Pt/FeO_x-300, (e) Pt/FeO_x-430, (f) Pt/FeO_x-500. Reaction conditions were as follows: 0.5% CO, 10% O_2/Ar balance, space velocity: 120000 mL·g^{-1}·h^{-1}.

Pt/FeO_x-300. Considering that the Pt loading amount is the same in these samples, the decrease should be correlated with the amount of hydroxides on the surface of FeO_x supports; i.e. the more amount of hydroxides, the more amount of Fe^{3+} species could be reduced. These Fe^{3+} species should be more active in the following CO oxidation reaction.

Role of FeO_x in the catalytic CO oxidation

The CO oxidation reaction was tested in a fixed-bed reactor system with a continuously flowing gas mixture of 0.5 vol % CO, 10 vol % O_2 and the balance Ar. The space velocity was fixed at 1.2×10^5 mL·g^{-1}·h^{-1}. Typically, the catalyst was directly used without any pretreatment. Fig. 10 shows profiles of the CO conversion as a function of the reaction temperature. Pt/FeO_x-100 could convert CO completely at room temperature (298 K), showing a high capability for CO oxidation. TOF of Pt/FeO_x-100 was 484×10^{-3} s^{-1} calculated based on surface Pt metal atoms. The surface Pt metal atoms measured from CO chemisorption is 1.54×10^{-5} mol•g_{cat}^{-1}. Other catalysts are less active than Pt/FeO_x-100 at room temperature. As for the samples of Pt/FeO_x-220, Pt/FeO_x-300 and Pt/FeO_x-500, the complete CO oxidations temperature in 10 vol % O_2/Ar is at *ca.* 80, 110 and 120 °C, respectively. It is evident that the catalytic activities of Pt/FeO_x catalysts decreased with the increase of treating temperature of FeO_x supports. Combined with above H_2-TPR results, it can confirm that the CO oxidation activities of Pt/FeO_x should depend on their redox properties. The difference of Pt/FeO_x redox properties should origin from the different states of FeO_x supports and Pt nanoparticles.[38]

In-situ DRIFT measurements were carried out to explore the possible reaction process of CO oxidation over Pt/FeO_x catalysts. The sample was first pretreated in Ar flow (20 mL·min^{-1}) for 20 min to remove the adsorbed water and oxygen molecular. The spectrum of pretreated sample was recorded as background. Using this background, the time-resolved spectra of Pt/FeO_x-100, Pt/FeO_x-300 and Pt/FeO_x-500 under different conditions were recorded (Fig. 11). As shown in Fig. 11A, the injection of CO on Pt/FeO_x-100 catalysts produces one band centered at 2067 cm^{-1}, which is attributed to the linear adsorption of CO on Pt centers.[39, 40] Meanwhile, A strong CO_2 peak can also be observed at around 2360 cm^{-1}. The appearance of

these peaks accompanies with the consumption peak of OH in the range of 3700 to 3300 cm^{-1}. This should be due to CO reacts with OH in this process. It could give direct evidence that OH groups on the surface of FeO_x-100 support participate in the CO oxidation. On the other hand, according to the ref 37, the band at about 3700 cm^{-1} is also a typical characterization of the redox process of FeO_x supports. It could reflect that the redox between Fe^{3+} and Fe^{2+} of the Pt/FeO_x catalyst occurs in the CO oxidation.

After switching to the flow of 20 vol % O_2/Ar (20 $mL \cdot min^{-1}$), the peaks assigned to the consumption of OH significantly decreased. This result shows that most of OH groups can be recovered during this process. But a weak signal still can be observed. The loss of small amount OH groups should be due to the participation of water in the recovery process, and the water should come from the crystal water of FeO_x-100 support. For confirming the role of water in the recovery of OH groups, stability tests over Pt/FeO_x-100 were carried out with and without water gas (Fig S6). A decrease of activity can be observed over Pt/FeO_x-100 after 200 min reaction without introducing water gas. As for reaction under a water gas flow, no change can be observed, indicating a high stability of Pt/FeO_x-100. Combined with above results, it shows that water should participate in the recovery process of OH groups.

Compared to Pt/FeO_x-100, the spectra of Pt/FeO_x-300 and Pt/FeO_x-500 change slightly in the range of 3700 to 3300 cm^{-1} after the injection of CO (Fig. 11B and C). This shows that the surface hydroxides of FeO_x-300 and FeO_x-500 support cannot react with CO directly at room temperature. It can be found that a few bands at 1519 and 1307 cm^{-1} appear obviously in the spectra of Pt/FeO_x-300 and Pt/FeO_x-500, which can be assigned to the carbonate-type species.[41,42] The spectra under the condition of co-presence of CO and O_2 were also detected on Pt/FeO_x-100, Pt/FeO_x-300 and Pt/FeO_x-500 catalysts. The band of the adsorbed CO is quite similar to that without O_2 (Fig. S7). It is known that the adsorption of O_2 on Pt sites could decrease back-donation of electron from Pt to CO.[39] This result shows that no competitive adsorption of O_2 occurred on the same Pt sites, suggesting that the CO oxidation on the Pt/FeO_x catalysts follows the noncompetitive mechanism. According to the above characterization data and analysis, it can be concluded that CO oxidation on these Pt/FeO_x catalysts should follow a redox mechanism.

For further confirming the role and the recoverability of OH groups in the CO oxidation, a series of verification experiment were carried out. A reference sample was obtained with a further treated FeO_x-100 (at 100 ^oC for 3 h) as a support. XRD patterns showed that the resultant support still possesses ferrihydrite phase (Fig. S8). The amount of surface OH groups decreased significantly compared with that of fresh FeO_x-100 (Fig. S9). The catalytic CO oxidation test shows that the resultant catalyst exhibits a much lower room-temperature activity compared with that of Pt/FeO_x-100 (Fig. S10). But its activity could be recovered in the presence of water vapour. Besides, we also observed that the catalytic activity of Pt/FeO_x-500 could be improved significantly when introducing water vapour into the reaction gas (Fig. S11). All these results confirm that surface OH groups play the important role of in the reaction. For understanding the importance of Pt^0 in the reaction, reductive (150°C, 5%H_2/Ar stream for 1 h) and oxidative (400°C, 20% O_2/Ar for 1 h) treatment was separately carried out on the sample of Pt/FeO_x-500. The trend of catalytic performance is that Pt/FeO_x-500 with reductive-treatment > Pt/FeO_x-500 > Pt/FeO_x-500 with oxidative-treatment (Fig. S12). It is known that the oxidation state of both Pt and FeO_x support might change during the treatment. From DRIFT spectra, the changes of surface OH groups FeO_x support could be ruled out (Fig. S13). The change of catalytic performance should be due to the changing of Pt active sites. It might imply that relatively large amount of Pt^0 should benefit to high catalytic performance.

As a high efficient Pt/FeO_x catalyst, the hydroxides on the iron oxide surface could participate in the CO oxidation, and then the supports supply sites for O_2 adsorption and activation. Pt provides

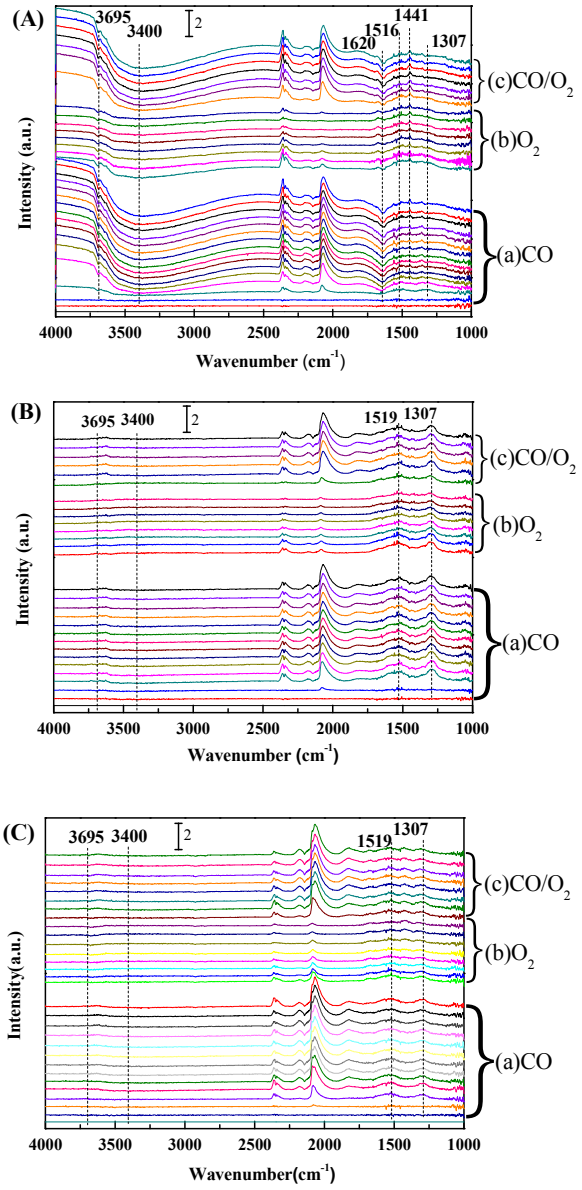

Fig. **11** In situ DRIFT spectra of Pt/FeOx catalysts: (A) Pt/FeOx-100, (B) Pt/FeOx-300, (C) Pt/FeOx-500 as a function of time after the gas flow was switched (a) from Ar to 1% CO/Ar, (b) from 1% CO/Ar to 20% O2/Ar, and (c) from 20% O2/Ar to CO/O2 at room temperature. Each spectrum was recorded with an interval of 40 s.

the sites for CO adsorption.[43] So, the valence of Pt species and the synergism between Pt and FeO_x support play key roles in determining the catalytic performance. It is known that the chemical bond between CO and Pt concerns the bonding 5σ and the antibonding 2π* orbitals of CO versus Pt orbitals.[44, 45] The 5σ-Pt interaction is electron-donating towards platinum and could strength the Pt-C bond. The antibonding 2π*-Pt interaction corresponds to an electron transfer from platinum to an antibonding CO orbital. Therefore, electron-rich Pt atoms could shift the Fermi level to a higher energy, and weaken the adsorption of CO through decreasing the strength of Pt-C bond. Besides, an increase of back-donation (increase of electron density in the 2π* orbital) could also lead to a weakening of the carbon-oxygen bond in the CO molecule.[39, 40, 46] Tuning this charge transfer between reagent and active centers could also improve the activation efficiency of CO oxidation. And this charge transfer should be significantly dependent on the surface charge density of catalysts. In our case, XPS results have shown that relatively large amounts of Pt^0 present in Pt/FeO_x-100 catalysts. In-situ DRIFT shows that the CO adsorption band of Pt/FeO_x-100 locates at lower wavenumber than that of Pt/FeO_x-300 and Pt/FeO_x-500 (see in Fig. S14). It shows that the strength of CO adsorption on Pt sites is relatively weak in Pt/FeO_x-100 catalyst, which might be another key factor responsible for the high activity of Pt/FeO_x-100 at room temperature.[47] The amount of surface hydroxides on FeO_x-100 is very important for obtaining large amounts of Pt^0 in Pt/FeO_x-100. The hydroxide groups endow the Pt/FeO_x-100 with an electron-rich surface. It could maximumly maintain the valence of Pt in the preparation process and construct efficient Pt-FeO_x interface. Combining the above characterization and analysis, the amount of hydroxides on the FeO_x, the valence of Pt and the synergism between Pt and hydroxide should be the determining factors for the performance of catalytic CO oxidation. These factors could be easily controlled using FeO_x with abundant surface hydroxide groups.

Conclusions

The correlation between the microstructure of FeO_x support and the CO oxidation performance of Pt/FeO_x catalyst has been investigated. It shows that FeO_x support possessing abundant surface hydroxides be suitable for preparing high performance Pt/FeO_x catalyst for low-temperature CO oxidation. Relatively large amounts of Pt^0 species can be preserved on the FeO_x support possessing abundant surface hydroxides. The surface hydroxides of FeO_x could also participate in the catalytic process. They could react with CO absorbed on Pt^0 sites and then recover easily in the co-presence of molecular oxygen and water gas. This work shows that FeO_x supports play an important role in the catalytic process by providing active sites and could affect the physic-chemical properties of Pt nanoparticles in the preparation process.

Acknowledgements

This work was supported by the National Science Foundation of China (Grant No. 21473073, 21473074 and 20973080), the Development Project of Science and Technology of Jilin Province (20130101014JC), the Fundamental Research Funds for the Central Universities and the Open Project of State Key Laboratory of Inorganic Synthesis and Preparative Chemistry.

Notes and references

1 A. Corma, P. Serna, P. Concepcion and J. J. Calvino, *J. Am. Chem. Soc.*, 2008, **130**, 8748-8753.
2 H. S. Wei, X. Y. Liu, A. Q. Wang, L. L. Zhang, B. T. Qiao, X. F. Yang, Y. Q. Huang, S. Miao, J. Y. Liu and T. Zhang, *Nat. Commun.*, 2014, **5**, 5634-5641.
3 K. Liu, A. Q. Wang and T. Zhang, *ACS Catal.*, 2012, **2**, 1165-1178.
4 C. B. Zhang, F. D. Liu, Y. P. Zhai, H. Ariga, N. Yi, Y. C. Liu, K. Asakura, M. Flytzani-Stephanopoulos and H. He, *Angew. Chem., Int. Ed.*, 2012, **51**, 9628-9632.
5 C. Pedrero, T. Waku and E. Iglesia, *J. Catal.*, 2005, **233**, 242-255.
6 A. Siani, O. S. Alexeev, G. Lafaye and M. D Amiridis, *J. Catal.*, 2009, **266**, 26-38.
7 A. Siani, B. Captain, O. S. Alexeev, E. Stafyla, A. B. Hungria, P. A. Midgley, J. M. Thomas, R. D. Adams and M. D Amiridis, *Langmuir*, 2006, **22**, 5160-5167.
8 K. Tanaka, M. Shou and Y. Z. Yuan, *J. Phys. Chem. C*, 2010, **114**, 16917-16923.
9 A. Bourane and D. Bianchi, *J. Catal.*, 2004, **222**, 499-510.
10 A. S. Ivanova, E. M. Slavinskaya, R. V. Gulyaev, V. I. Zaikovskii, O. A. Stonkus, I. G. Danilova, L. M. Plyasova, I. A. Polukhina and A. I. Boronin, *Appl. Catal., B*, 2010, **97**, 57-71.
11 J. Singh and J. A. van Bokhoven. *Catal. Today*, 2010, **155**, 199-205.
12 Q. Fu, W. X. Li, Y. X. Yao, H. Y. Liu, H. Y. Su, D. Ma, X. K. Gu, L. M. Chen, Z. Wang, H. Zhang, B. Wang and X.H. Bao, *Science*, 2010, **328**, 1141-1144.
13 M. Cargnello, V. V. T. Doan-Nguyen, T. R. Gordon, R. E. Diaz, E. A. Stach, R. J. Gorte, P. Fornasiero and C. B. Murray, *Science*, 2013, **341**, 771-773.
14 K. An, S. Alayoglu, N. Musselwhite, S. Plamthottam, G. Melaet, A. E. Lindeman and G. A. Somorjai, *J. Am. Chem. Soc.*, 2013, **135**, 16689-16696.
15 O. Korotkikh and R. Farrauto, *Catal. Today*, 2000, **62**, 249-254.
16 X. S. Liu, O. Korotkikh and R. Farrauto, *Appl. Catal., A*, 2002, **226**, 293-303.
17 M. Shou, K. -I. Tanaka, K. Yoshioka, Y. Moro-oka and S. Nagano, *Catal. Today*, 2004, **90**, 255-261.
18 S. Y. Li, G. Liu, H. L. Lian, M. J. Jia, G. M. Zhao, D. Z. Jiang and W. X. Zhang, *Catal. Commun.*, 2008, **9**, 1045-1049.
19 L. Q. Liu, F. Zhou, L. G. Wang, X. J. Qi, F. Shi and Y. Q. Deng, *J. Catal.*, 2010, **274**, 1-10.
20 B. T. Qiao, A. Q. Wang, X. F. Yang, L. F. Allard, Z. Jiang, Y. T. Cui, J. Y. Liu, J. Li and T. Zhang, *Nat. Chem.*, 2011, **3**,634-641.
21 N. H. An, S. Y. Li, P. N. Duchesne, P. Wu, W. L. Zhang, J. -F. Lee, S. Cheng, P. Zhang, M. J. Jia and W. X. Zhang, *J. Phys. Chem. C*, 2013, **117**, 21254-21262.
22 G. X. Chen, Y. Zhao, G. Fu, P. N. Duchesne, L. Gu, Y. P. Zheng, X. F. Weng, M. S. Chen, P. Zhang, C. -W. Pao, J. -F. Lee and N. F. Zheng, *Science*, 2014, **344**, 495-499.
23 A. Tomita, K. -I. Shimizu, K. Kato, T. Akita and Y. Tai, *J. Phys. Chem. C*, 2013, **117**, 1268-1277.
24 J. Lin, B. T. Qiao, J. Y. Liu, Y. Q. Huang, A. Q. Wang, L. Li, W. S. Zhang, L. F. Allard, X. D. Wang and T. Zhang, *Angew. Chem. Int. Ed.*, 2012, **51**, 2920-2924.
25 Y. Wang, J. W. Ren, K. Deng, L. L. Gui and Y. Q. Tang, *Chem. Mater.*, 2000, **12**, 1622-1627.

26 J. L. Jambor and J. E. Dutrizac. *Chem. Rev.*, 1998, **98**, 2549-2585.
27 M. Hermanek, R. Zboril, I. Medrik, J. Pechousek and C. Gregor, *J. Am. Chem. Soc.*, 2007, **129**, 10929-10936.
28 H. Tüysüz, E. L. Salabas, C. Weidenthaler and F. Schüth, *J. Am. Chem. Soc.*, 2008, **130**, 280-287.
29 K. Raja, P. S. Ramesh and D. Geetha, *Spectrochim. Acta, Part A.*, 2014, **131**, 183-188.
30 S. F. Parker, *Chem. Commun.*, 2011, **47**, 1988-1990.
31 B. J. Tan, K. J. Klabunde and P. M. A. Sherwood, *Chem. Mater.*, 1990, **2**, 186-191.
32 L. S. Xu, W. H. Zhang, Y. L. Zhang, Z. F. Wu, B. H. Chen, Z. Q. Jiang, Y. S. Ma, J. L. Yang and W. X. Huang, *J. Phys. Chem. C*, 2011, **115**, 6815-6824.
33 B. T. Qiao, A. Q. Wang, L. Li, Q. Q. Lin, H. S. Wei, J. Y. Liu and T. Zhang, *ACS Catal.*, 2014, **4**, 2113-2117.
34 Z. F. Zheng, J. Teo, Xi. Chen, H. W. Liu, Y. Yuan, E. R. Waclawik, Z. Y. Zhong and H. Y. Zhu, *Chem. Eur. J.*, 2010, **16**, 1202-1211.
35 R. Ahmadi, M. K. Amini and J. C. Bennett, *J. Catal.*, 2012, **292**, 81-89.
36 Z. Z. Yang, Na. Zhang, Yi. Cao, M. C. Gong, M. Zhao and Y. Q. Chen, *Catal. Sci. Technol.*, 2014, **4**, 3032-3043.
37 L. Li, A. Q. Wang, B. T. Qiao, J. Lin, Y. Q. Huang, X. D. Wang and T. Zhang, *J.Catal.*, 2013, **299**, 90-100.
38 K. F. Zhao, H. L. Tang, B. T. Qiao, L. Li and J. H. Wang, ACS Catal., 2015, **5**, 3528-3539.
39 P. -A. Carlsson, L. Osterlund, P. Thormahlen, A. Palmqvist, E. Fridell, J. Jansson and M. Skoglundh, *J. Catal.*, 2004, **226**, 422-434.
40 P. Gruene, A. Fielicke, G. Meijer and D. M. Rayner, *Phys. Chem. Chem. Phys.*, 2008, **10**, 6144-6149.
41 J. Lin, B. T. Qiao, L. Li, H. L. Guan, C. Y. Ruan, A. Q. Wang, W. S. Zhang, X. Wang and T. Zhang, *J. Catal.*, 2014, **319**, 142-149.
42 K. I. Tanaka, M. Shou, H. He, X. Y. Shi and X. L. Zhang, *J. Phys. Chem. C*, 2009, **113**, 12427-12433.
43 S. Y. Li, M. J. Jia, J. Gao, P. Wu, M. L. Yang, S. H. Huang, X. W. Dou, Y. Yang and W. X. Zhang, *J. Phys. Chem. C*, 2015, **119**, 2483-2490.
44 G. Blyholder, *J. Phys. Chem.*, 1975, **79**, 756-761.
45 G. Blyholder, *J. Phys. Chem.*, 1964, **68**, 2772-2777.
46 P. Bazin, O. Saur, J. C. Lavalley, M. Daturi and G. Blanchard, *Phys. Chem. Chem. Phys.*, 2005, **7**, 187-194.
47 O. Pozdnyakova, D. Teschner, A. Wootsch, J. Kröhnert, B. Steinhauer, H. Sauer, L. Toth, F. C. Jentoft, A. Knop-Gericke, Z. Paál and R. Schlögl, *J. Catal.*, 2006, **237**, 1-16.

Graphical Abstract

Role of FeO_x support in constructing high performance Pt/FeO_x catalyst for low-temperature CO oxidation

Bin Zheng,[a] Gang Liu*,[a] Longlong Geng,[a] Junyan Cui,[a] Shujie Wu,[a] Ping Wu,[a] Mingjun Jia,[a] Wenfu Yan[b] and Wenxiang Zhang*[a]

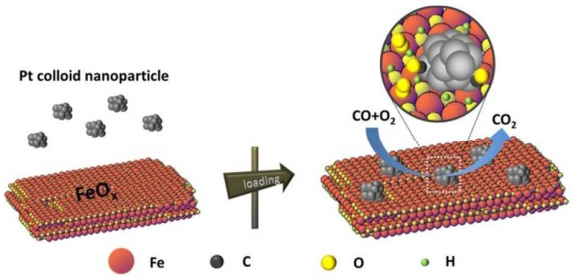

FeO_x support not only affects the oxidation state of Pt nanoparticles, but also provides active sites in the catalytic process.